

NANO COMMENTARY

Open Access



Nanostructured Polyphase Catalysts Based on the Solid Component of Welding Aerosol for Ozone Decomposition

Tatyana Rakitskaya¹, Alla Truba^{1,2*}, Alim Ennan² and Vitaliya Volkova¹

Abstract

Samples of the solid component of welding aerosols (SCWAs) were obtained as a result of steel welding by ANO-4, TsL-11, and UONI13/55 electrodes of Ukrainian manufacture. The phase compositions of the samples, both freshly prepared (FP) and modified (M) by water treatment at 60 °C, were studied by X-ray phase analysis and IR spectroscopy. All samples contain magnetite demonstrating its reflex at $2\theta \sim 35^\circ$ characteristic of cubic spinel as well as manganochromite and iron oxides. FP SCWA-TsL and FP SCWA-UONI contain such phases as CaF_2 , water-soluble fluorides, chromates, and carbonates of alkali metals. After modification of the SCWA samples, water-soluble phases in their composition are undetectable. The size of magnetite nanoparticles varies from 15 to 68 nm depending on the chemical composition of electrodes under study. IR spectral investigations confirm the polyphase composition of the SCWAs. As to IR spectra, the biggest differences are apparent in the regions of deformation vibrations of M–O–H bonds and stretching vibrations of M–O bonds (M–Fe, Cr). The catalytic activity of the SCWAs in the reaction of ozone decomposition decreases in the order SCWA-ANO > SCWA-UONI > SCWA-TsL corresponding to the decrease in the content of catalytically active phases in their compositions.

Keywords: Welding aerosol, Solid component, Characterization, Ozone decomposition, Air purification

Background

Welding aerosols consisting of solid and gaseous components are evolved as a result of complex physical and chemical processes taking place in welding. The solid component of welding aerosol (SCWA) is the air-dispersed particulate formed out of the welding arc in consequence of the oxidation and condensation of vapors of components of electrode coatings, welding fluxes, and metals. The gaseous component of welding aerosol (GCWA) is a result of complex reactions leading to the formation of HF, SiF_4 , NO_x , and O_3 [1, 2]. Ozone is one of the most hazardous among the listed gases: its maximum permissible concentration is 0.1 mg/m^3 . Taking into consideration volumes and technologies of welding and related industries as well as materials used for them, it is

important not only to decrease the toxic effect of SCWAs and GCWAs on the environment and operating personnel but also to recycle solid wastes in order to obtain industrial products.

As appears from literature, chemical and phase compositions of SCWAs depend on a nature of weld metals and electrodes, materials of electrode coatings, and welding conditions [2–12]. Our investigations show that magnetite and manganochromite contained in compositions of SCWAs formed in the process of steel welding by some electrodes manufactured in Ukraine exhibit stable catalytic behavior in the reaction of ozone decomposition for the wide range of ozone concentrations ($1\text{--}100 \text{ mg/m}^3$) [13, 14]. It can be expected that an increase in concentrations of catalytically active phases in SCWAs obtained as a result of removing impurity phases and phases inactive in the reaction of ozone decomposition would lead to a change in kinetic and stoichiometric parameters of the reaction.

* Correspondence: truba@onu.edu.ua

¹Odessa I.I. Mechnikov National University, 2 Dvoryanskaya str., Odessa 65082, Ukraine

²Physicochemical Institute of Environment and Human Protection, 3, Preobrazhenskaya St., Odessa 65082, Ukraine

As follows from literary data [15–18], nanoparticles of magnetite (FeFe_2O_4) and its metal-substituted forms (MFe_2O_4) are prepared by their precipitation in an aqueous medium at temperatures not exceeding 60 °C. Such a treatment of SCWAs with water at the mentioned temperature can be used also as a mild technique not leading to structural changes in magnetite and its metal-substituted forms.

The aim of the work is to compare the phase compositions of freshly prepared and modified samples of the SCWAs obtained as a result of steel welding with the help of electrodes differing by their chemical compositions and to determine the catalytic activity of the SCWAs in the reaction of ozone decomposition.

Materials and Methods

The welding fume fractions of the SCWAs with an aerodynamic diameter of $\leq 1 \mu\text{m}$ formed in the process of metal arc welding by 3-mm-diameter electrodes with either rutile (ANO-4 (ISO 2560 E432R 21)) or carbonate-fluorite (TsL-11 (ISO E19.9NbB20) and UONI 13/55 (ISO 2560 E434B20)) electrode coatings were selected for the study. Welding was performed under conditions of positive current, reverse polarity, $U = 33 \text{ V}$, $I = 140\text{--}150 \text{ A}$, and the welding speed of 4.5 mm/s [2, 3]. Elemental analysis of the two SCWAs showed that both predominantly consisted of iron and manganese, and SCWA-TsL-11 was characterized by a much higher content of chromium and nickel [3].

In order to prepare modified samples, 20 mL of distilled water was added to 1 g of a SCWA sample and the suspension obtained was kept at 60 °C for 2 h under continuous stirring. After that, the particulate was filtered and dried at 110 °C till constant weight.

SCWA samples were characterized by X-ray diffraction phase analysis and IR spectroscopy. In addition, they were tested in the reaction of low-temperature ozone decomposition.

The samples were identified based on X-ray diffraction phase analysis data recorded on a Siemens D500 diffractometer (CuK_α radiation, $\lambda = 1.54178 \text{ \AA}$) with a secondary beam graphite monochromator. The phases were identified with the help of International Centre for Diffraction Data (ICDD) PDF-1 databases provided as a part of the Siemens D500 diffractometer software.

Infrared analysis was carried out using a Perkin Elmer FT-IR spectrometer with a resolution of 4 cm^{-1} ; pellets consisting of 1 mg of the material under study and 200 mg of KBr were compressed under pressure of 7 tons/ cm^2 for 30 s.

The catalyst samples (0.5 g) were tested using a gas-flow setup with a fixed bed reactor at 20 °C, relative humidity of 65 %, and the linear velocity (u) of an ozone-air mixture (OAM) equal to 3.2 cm/s. The

ozone decomposition was monitored by measuring the final ozone concentration ($C_{\text{O}_3}^f$). The initial ozone concentration ($C_{\text{O}_3}^{\text{in}} = 100 \text{ mg/m}^3$) and $C_{\text{O}_3}^f$ were measured by a Tsycon-Reverse optical analyzer with a detection limit of 1 mg/m^3 . The reaction rate (W) calculations based on the data of ozone concentration changing after OAM passing through the static bed of the catalyst were made using the following equation:

$$W = \frac{\omega(C_{\text{O}_3}^{\text{in}} - C_{\text{O}_3}^f)}{m_s}, \text{ mol}/(\text{g} \times \text{s}), \quad (1)$$

where $\omega = 1.67 \times 10^{-2}$ is the OAM volume flow rate, L/s; $C_{\text{O}_3}^{\text{in}}$ and $C_{\text{O}_3}^f$ are the initial and final ozone concentrations in the OAM, respectively, mol/L; and m_s is the mass of the catalyst sample, g.

The reaction rate values measured after 1 min of OAM passing named as the initial reaction rate, W_{in} , were used to characterize the process.

The first-order reaction rate constant with reference to ozone, k_1 , was graphically calculated using the following equation:

$$k_1 = \frac{1}{\tau} \ln \frac{C_{\text{O}_3}^{\text{in}}}{C_{\text{O}_3}^f}, \text{ s}^{-1}, \quad (2)$$

where τ is reaction time, s.

The reaction rate constant, $k_{1/2}$, was quantified for the half-conversion time, $\tau_{1/2}$, i.e., for the moment of time when the degree of ozone decomposition became equal to 50 %, as follows:

$$k_{1/2} = \frac{0.69}{\tau_{1/2}}, \text{ s}^{-1}. \quad (3)$$

The amount of ozone entered into the reaction up to the moment of experiment termination (Q_{exp} , moles of O_3) was calculated as the square of the corresponding ozonogram plotted as ΔC_{O_3} vs. τ function.

Discussion

XRD Characterization

X-ray diffraction patterns of freshly prepared (Fig. 1a, c, e) and modified (Fig. 1b, d, f) SCWA samples show a substantial difference in positions, intensities, and numbers of reflections; however, all of them are characterized by a high degree of crystallinity.

Tables 1, 2, and 3 show results of analysis of our data related to the phase composition of samples under study and their X-ray spectral parameters: angles of reflection, 2θ ; interplanar spacings, d (\AA), both experimental and reference; and normalized intensities, I_N . Taking into account the chemical composition of both electrode wires and electrode coatings, identifying phases in SCWA

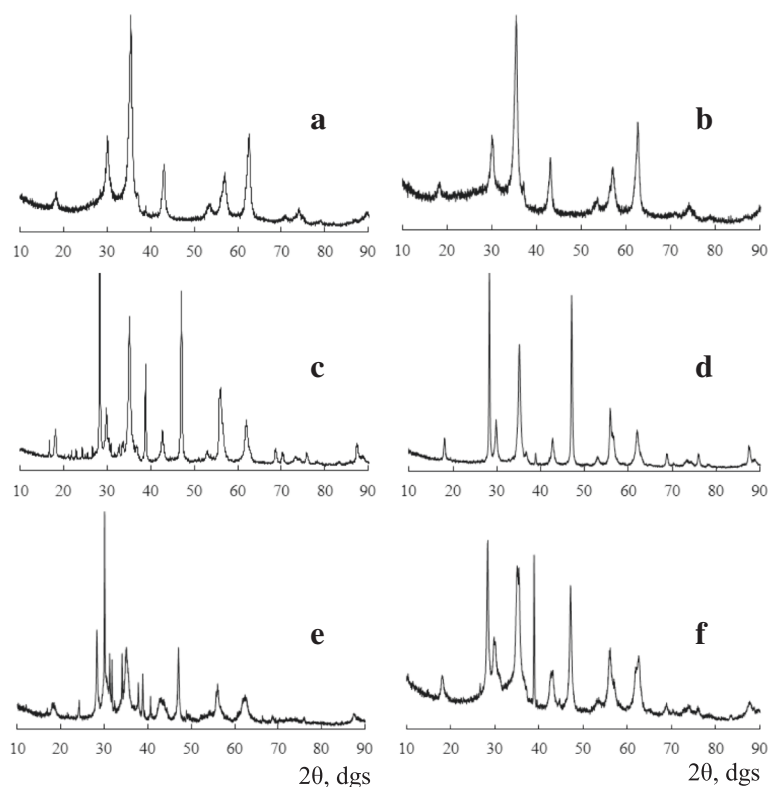


Fig. 1 X-ray diffraction patterns of freshly prepared (**a, c, e**) and modified (**b, d, f**) SCWAs: **a, b** ANO; **c, d** TsL; **e, f** UONI

compositions, we considered the possibility of a formation of various spinels, intermetallic compounds, metal oxides, fluorides, silicate forms, carbonates, etc. Since superposition of reflections occurs in many cases, we must pay first-priority attention to the presence of individual reflections of each phase in the X-ray spectra. As can be seen from Tables 1, 2, and 3, the SCWA samples are poly-phase. Seven crystalline phases, i.e., magnetite (Fe_3O_4) [ICPDS 19-0629], manganochromite ($(\text{Mn,Fe})(\text{Cr,V})_2\text{O}_4$) [ICPDS 31-0630], manganese oxide (Mn_3O_4) [ICPDS 13-0162], carbonates of potassium (K_2CO_3) and sodium (Na_2CO_3) [19], potassium chromate (K_2CrO_4), and dichromate $\text{K}_2\text{Cr}_2\text{O}_7$ [19], have been identified in freshly prepared (FP) SCWA-ANO (Table 1). Phase compositions of FP SCWA-TsL (Table 2) and FP SCWA-UONI (Table 3) are more complicated. In addition to the phases found in the first sample (Table 1), iron oxides ($\beta\text{-Fe}_2\text{O}_3 \cdot \text{H}_2\text{O}$ and Fe_2O_3) [19], calcium fluoride (CaF_2) [ICPDS 35-0816], and magnesium silicate (MgSiO_3) [ICPDS 11-0273] have been identified. The most intense reflections were observed for phase mixtures.

For modified (M) SCWAs, the analysis of X-ray diffraction patterns (Fig. 1b, d, f) and the information presented in Tables 1, 2, and 3 show a decrease in the number of reflections and a change in their intensity ratios due to the loss of water-soluble phases. M SCWAs

contain phases catalytically active in redox reactions (CAP) such as magnetite, manganochromite, iron oxides, and their mixtures. Taking into account integral intensities of the corresponding reflections, the content (%) of CAPs could be estimated for each SCWA sample (Table 4). It decreases in the order SCWA-ANO > SCWA-UONI > SCWA-TsL. Judging from the peak at $2\theta \sim 35^\circ$ (311), all SCWA samples contain magnetite in the form of ferrites with a cubic spinel structure [10, 20–27]. Based on this fact, we have estimated the unit cell parameter (a). The values of a parameter obtained by us (Table 4) are in agreement with literature ones for the cubic unit cell parameter of FeFe_2O_4 , i.e., 8.380 Å [23], 8.199 Å [24], and 8.394 Å [25]. Slight differences in the literature values can be caused by differences in techniques used for ferrite preparation. For metal-substituted ferrites, $(\text{Zn,Mn})\text{Fe}_2\text{O}_4$, a is in the range from 8.459 to 8.472 Å [28].

Using the well-known Scherrer equation, the sizes of magnetite nanoparticles (D , nm) were estimated based on the breadth at half-peak height of the X-ray diffraction (XRD) line corresponding to (311) reflections for the freshly prepared and modified SCWA samples (Table 4). It can be seen that the sizes of magnetite nanoparticles depend, other things being equal, on the chemical composition of electrodes and the highest D

Table 1 X-ray spectral parameters and the phase composition of SCWA-ANO

Phase Ref.	Freshly prepared sample				Modified sample			
	$2\theta, ^\circ$	I_N	d (Å)		$2\theta, ^\circ$	I_N	d (Å)	
			Exp.	Ref.			Exp.	Ref.
(Mn,Fe)(Cr,V) ₂ O ₄	18.212	85	4.867	4.85	18.362	219	4.828	4.85
	36.654	70	2.449	2.44	–	–	–	–
	–	–	–	–	42.784	210	2.112	2.12
	56.402	121	1.630	1.63	56.453	197	1.629	1.63
	61.727	149	1.502	1.50	–	–	–	–
	–	–	–	–	62.402	369	1.487	1.50
Fe ₃ O ₄	35.389	1000	2.534	2.55	35.546	999	2.524	2.55
	36.978	87	2.429	2.42	37.204	222	2.415	2.42
	43.027	297	2.100	2.10	43.186	344	2.093	2.10
	53.414	58	1.714	1.71	–	–	–	–
	57.001	219	1.614	1.61	57.015	295	1.614	1.61
	62.587	463	1.483	1.483	62.724	528	1.480	1.483
	73.957	75	1.281	1.279	74.154	121	1.278	1.279
	79.004	22	1.211	1.210	78.943	70	1.212	1.210
Mn ₃ O ₄	53.638	57	1.707	1.70	53.712	147	1.705	1.70
K ₂ CO ₃	34.189	95	2.620	2.61	Not detected			
Na ₂ CO ₃	56.058	90	1.639	1.62	Not detected			
	62.071	250	1.494	1.48	Not detected			
	63.278	62	1.470	1.48	Not detected			
K ₂ CrO ₄	38.826	38	2.317	2.32	Not detected			
K ₂ Cr ₂ O ₇	30.809	75	2.900	2.85	Not detected			
	53.091	48	1.724	1.73	Not detected			
(Mn,Fe)(Cr,V) ₂ O ₄ ;	30.033	328	2.973	2.99	30.159	439	2.961	2.99
Fe ₃ O ₄ ;				2.97				2.97
K ₂ CrO ₄				2.96				2.96

values are for the SCWA-UONI samples. It should be noted that, despite the significant differences in D values presented in Table 4, it does not contradict with the data spread reported in literature [10, 25–27, 29, 30]. Depending on techniques and conditions of magnetite preparation used in those works, D values vary from 11 to 52 nm.

IR Characterization

The difficulties in differentiation of mixed and individual characteristic vibrations of M–O and M–OH bonds (M—metal) make IR spectral investigations of polyphase systems, specifically SCWAs, very complicated. The data obtained in our earlier work [14] for freshly prepared SCWA-ANO and SCWA-TsL show that the biggest differences are observed in the region of 1700–400 cm⁻¹. Therefore, Fig. 2 shows only that spectral region for the freshly prepared (panels a, c, e) and modified

(panels b, d, f) SCWA samples. As can be seen, the bands characterizing deformation vibrations of water molecules in the freshly prepared samples are not simple that indicates energy inhomogeneity of surface sites occupied by water molecules.

For identification of characteristic vibration frequencies of M–O and M–OH bonds in the IR spectra, literary data for both metal oxides [28, 31–33] and spinels [21–24, 34, 35] whose compositions are similar to those determined in the SCWAs by X-ray phase analysis were used. IR spectra of the freshly prepared SCWA samples (Fig. 2a, c, e) contain many absorption bands of different intensity and resolution that confirms the structural-phase inhomogeneity of the samples. An intense complex-shaped band is detected in the spectral region of 1250–850 cm⁻¹ for FP SCWA-ANO. Its components at 1043 and 1023 cm⁻¹ can be assigned to deformation vibrations of Fe–O–H bonds in spinel whereas absorption bands at 1004, 986, 967, and 948 cm⁻¹ can be

Table 2 X-ray spectral parameters and the phase composition of SCWA-TsL

Phase	Freshly prepared sample				Modified sample			
	$2\theta, ^\circ$	I_N	d (Å)		$2\theta, ^\circ$	I_N	d (Å)	
			Exp.	Ref.			Exp.	Ref.
(Mn,Fe)(Cr,V) ₂ O ₄	18.072	122	4.905	4.89	18.179	102	4.876	4.89
	36.685	50	2.448	2.44	36.766	52	2.442	2.44
Fe ₃ O ₄	35.095	658	2.555	2.55	35.201	567	2.548	2.55
	43.104	48	2.097	2.10	43.113	59	2.097	2.10
	73.622	24	1.286	1.279	73.675	30	1.285	1.279
β -Fe ₂ O ₃ ·H ₂ O	46.383	37	1.956	1.96	46.077	16	1.968	1.96
	68.297	16	1.372	1.38	68.798	71	1.363	1.38
Mn ₃ O ₄	73.876	21	1.282	1.28	73.315	33	1.290	1.28
	78.794	11	1.214	1.21	78.534	13	1.217	1.21
	89.748	11	1.092	1.09	89.418	17	1.095	1.09
CaF ₂	46.999	871	1.932	1.93	47.130	881	1.927	1.93
	68.647	76	1.365	1.365	68.798	271	1.363	1.365
	87.378	113	1.115	1.115	87.531	118	1.114	1.115
MgSiO ₃	30.804	50	2.900	2.908	30.628	22	2.917	2.900
	61.330	49	1.510	1.499	61.513	60	1.506	1.499
K ₂ CO ₃	31.670	11	2.822	2.80	Not detected			
K ₂ CrO ₄	29.249	47	3.051	3.07	Not detected			
	30.310	83	2.946	2.96	Not detected			
CaF ₂ ;MgSiO ₃	28.251	1000	3.156	3.154	28.386	999	3.142	3.154
				3.170				3.170
K ₂ CO ₃	34.486	117	2.599	2.61	Not detected			
Na ₂ CO ₃				2.60				
K ₂ CrO ₄ ;NaF; β -Fe ₂ O ₃ ·H ₂ O	38.802	455	2.319	2.321	38.910	49	2.313	2.29
				2.32				2.32
				2.29				2.29
(Mn,Fe)(Cr,V) ₂ O ₄ ; β -Fe ₂ O ₃ ·H ₂ O;Fe ₃ O ₄ ;KF·2H ₂ O	42.631	147	2.119	2.12	42.747	123	2.114	2.12
				2.10				2.10
				2.10				2.10
				2.12				2.12
(Mn,Fe)(Cr,V) ₂ O ₄ ; β -Fe ₂ O ₃ ·H ₂ O;KF·2H ₂ O	61.969	200	1.496	1.50	62.051	173	1.495	1.50
				1.494				1.494
				1.495				1.495
				1.482				1.482
Fe ₃ O ₄ ; β -Fe ₂ O ₃ ·H ₂ O;Fe ₃ O ₄ ;Na ₂ CO ₃	62.361	97	1.487	1.483	62.471	88	1.485	1.483
				1.485				1.485
				1.486				1.486
				1.482				1.482

attributed to stretching vibrations of Cr–O bonds in the case of a coordinatively unsaturated chromium atom. A low-intensity band at 1269 cm⁻¹ is assigned to vibrations of a Fe–O–H bond in spinel. Intense bands at 598 and 582 cm⁻¹ as well as moderate-intensity bands at 458 and 436 cm⁻¹ are caused by vibrations of Fe–O bonds in the

case of iron cations located in tetrahedral and octahedral positions of a spinel structure. For FP SCWA-TsL, deformation vibrations of a Fe–O–H bond in spinel are detected at 1094, 1074, 1046, and 1026 cm⁻¹ as very weak unassisted bands separated from one another by intervals of 20 cm⁻¹. A similar series of bands was observed in the

Table 3 X-ray spectral parameters and the phase composition of SCWA-UONI

Phase	Freshly prepared sample				Modified sample			
	$2\theta, ^\circ$	I_N	$d, \text{Å}$		$2\theta, ^\circ$	I_N	$d, \text{Å}$	
			Exp.	Ref.			Exp.	Ref.
(Mn,Fe)(Cr,V) ₂ O ₄	18.055	54	4.909	4.89	18.068	144	4.906	7.89
	29.740	131	3.001	2.99	29.797	299	2.996	2.99
	–	–	–	–	42.425	168	2.129	2.12
	56.066	160	1.639	1.63	56.130	310	1.637	1.639
	61.823	95	1.499	1.50	61.806	257	1.50	1.50
Fe ₃ O ₄ (magnetite)	35.465	177	2.529	2.53	35.418	726	2.532	2.53
	42.880	89	2.107	2.10	42.899	206	2.106	2.10
	–	–	–	–	56.837	134	1.619	1.61
	62.104	111	1.486	1.48	62.403	316	1.487	1.485
Fe ₂ O ₃ (goethite, hematite)	24.103	44	3.689	3.68	–	–	–	–
	35.844	87	2.503	2.51	35.961	174	2.495	2.51
	62.134	106	1.493	1.485	62.137	266	1.493	1.485
β -Fe ₂ O ₃ ·H ₂ O (agacansite)	39.243	31	2.293	2.29	39.502	25	2.280	2.29
	43.055	92	2.099	2.10	43.112	213	2.097	2.10
Mn ₃ O ₄	28.749	66	3.103	3.08	–	–	–	–
	42.664	88	2.117	2.10	42.634	215	2.119	2.10
	62.689	103	1.481	1.48	62.557	339	1.484	1.48
CaF ₂	28.282	357	3.153	3.15	28.319	1000	3.149	3.15
	47.023	317	1.931	1.93	47.075	751	1.929	1.93
	68.663	31	1.366	1.365	68.546	54	1.368	1.365
	87.361	55	1.115	1.115	87.303	69	1.116	1.115
K ₂ CO ₃	31.768	208	2.815	2.80	Not detected			
	37.831	141	2.376	2.37	Not detected			
Na ₂ CO ₃ ·H ₂ O	40.628	95	2.220	2.24	Not detected			
K ₂ CrO ₄	29.176	40	3.058	3.07	Not detected			
	53.028	23	1.726	1.72	Not detected			
	57.110	39	1.612	1.61	Not detected			
MgSiO ₃	30.844	109	2.897	2.908	30.672	94	2.912	2.908
	54.978	27	1.669	1.66	55.266	57	1.660	1.66
	68.914	16	1.361	1.359	68.852	68	1.362	1.359
Fe ₃ O ₄ ;Mn ₃ O ₄ ;K ₂ CrO ₄ ;Na ₂ CO ₃	30.073	1000	2.969	2.97	30.046	268	2.972	2.97
				2.98				2.98
				2.96				2.96
				2.96				2.96
K ₂ Cr ₂ O ₇ ;Mn ₃ O ₄	31.224	239	2.862	2.87	31.090	64	2.874	2.87
				2.87				2.87
K ₂ CO ₃ ;β-Fe ₂ O ₃ ·H ₂ O	34.090	255	2.628	2.61	33.914	58	2.671	2.61
(Mn,Fe)(Cr,V) ₂ O ₄ ;β-Fe ₂ O ₃ ·H ₂ O;MgSiO ₃	35.050	279	2.558	2.55	35.031	775	2.559	2.55
				2.55				2.55
				2.551				2.551
β-Fe ₂ O ₃ ·H ₂ O;Mn ₃ O ₄ ;K ₂ CrO ₄ ;NaF	38.836	184	2.317	2.29	38.854	800	2.316	2.29

Table 3 X-ray spectral parameters and the phase composition of SCWA-UONI (Continued)

				2.36				2.36
				2.32				2.32
				2.32				2.32
$\beta\text{-Fe}_2\text{O}_3\cdot\text{H}_2\text{O};\text{CaF}_2;\text{MgSiO}_3$	55.760	130	1.647	1.648	55.941	340	1.642	1.648
				1.647				1.647
				1.642				1.642

spectrum of $(\text{Zn,Mn})\text{Fe}_2\text{O}_4$ spinel [28]. For the FP SCWA-TsL sample, a distinctive feature of its spectrum is a clear-cut resolution of the bands at 945 and 886 cm^{-1} assigned to stretching vibrations of Cr–O when the chromium atom is coordinatively saturated [32]. An intense band centered at 597 cm^{-1} with a shoulder at 615 cm^{-1} is a combined one and corresponds to vibrations of Fe–O bonds in both a spinel structure and free iron(III) oxides. Deformation vibrations of a Fe–O–H bond in a spinel structure of FP SCWA-UONI are detected as high-resolution low-intensity bands at 1275 and 1116 cm^{-1} with a shoulder at 1052 cm^{-1} . Compared with the spectra of other freshly prepared SCWAs, the spectrum of FP SCWA-UONI has some differences in the region of Cr–O stretching vibrations. They appear in the composition of a combined band having its maximum at 1007 and a shoulder at 984 cm^{-1} and also in the appearance of a sharp band at 832 cm^{-1} . Some absorption bands detected in the region of 800–400 cm^{-1} are assigned to stretching vibrations of Fe–O–H bonds: 597 and 490 cm^{-1} —in spinels—and 701, 613, 588, and 419 cm^{-1} —in individual iron(III) oxides.

Figure 2 shows IR spectral fragments covering the region of 1800–400 cm^{-1} for M SCWA-ANO (panel b), M SCWA-TsL (panel d), and M SCWA-UONI (panel f). It can be seen that the modification results in some structural-phase changes. In the spectral region corresponding to deformation vibrations of water molecules, only one band is detected for each sample: 1634 cm^{-1} for M SCWA-ANO, 1637 cm^{-1} for M SCWA-TsL, and 1633 cm^{-1} for M SCWA-UONI. As expected, the biggest changes take place in the region of 1250–850 cm^{-1}

which belongs to deformation vibrations of M–O–H bonds most sensitive to changes in spinel structures [28]. For example, for M SCWA-ANO, a moderate-intensity band appeared at 1027 cm^{-1} (Fe–OH) instead of the intense complex-shaped band detected in the spectral region of 1250–850 cm^{-1} for FP SCWA-ANO. Absorption bands assigned to Cr–O stretching vibrations do not appear independently in the M SCWA-ANO spectrum because of a low chromium content. Most likely, these bands are superposed with a more intense band characteristic for a Fe–OH bond in spinel. In the M SCWA-TsL spectrum, a broad band centered at 1050 cm^{-1} with shoulders at 1096, 1070, and 1024 cm^{-1} can be attributed to stretching vibrations of a Fe–OH bond in spinel, and individual bands at 945 and 889 cm^{-1} do not disappear nor shift due to a high chromium content in the electrode. Substantial changes are observed in the spectral region of 1250–850 cm^{-1} for M SCWA-UONI. A combined band located there broadens, and 1136, 1061, 1045, and 1029 cm^{-1} frequencies in its high-frequency component are assigned to Fe–O–H vibrations in spinel whereas a 1003 cm^{-1} frequency located in its low-frequency component is attributed to the vibration of a Cr–O bond. The intensity of a band at 832 cm^{-1} markedly decreases. Two bands, the first one centered at 587 cm^{-1} with a shoulder at 709 cm^{-1} and the second one located at 464 cm^{-1} , are caused by vibrations of Fe–O bonds with iron cations disposed in tetrahedral and octahedral positions in a spinel structure.

Table 4 CAP contents, unit cell parameters, and sizes of magnetite nanoparticles estimated from (311) reflection of Fe_3O_4

Sample	Content of CAP, %	a , Å	D , nm
FP SCWA-ANO	81	8.404	18.0
M SCWA-ANO	97	8.371	15.0
FP SCWA-TsL	51	8.474	23.0
M SCWA-TsL	52	8.451	20.5
FP SCWA-UONI	54	8.388	68.0
M SCWA-UONI	78	8.398	31.5

Testing SCWA Samples in the Reaction of Ozone Decomposition

Figure 3 shows time dependences of the final ozone concentration, $C_{\text{O}_3}^f$, in the course of ozone decomposition by the freshly prepared (panel a) and modified (panel b) SCWA samples.

As can be seen, the duration of the reaction and profiles of kinetic curves depend on phase compositions of the samples and the longest reaction time is observed for FP SCWA-ANO. Initial portions of the kinetic curves are most sensitive to alterations in SCWA compositions. During the first 10 min, $C_{\text{O}_3}^f$ values increase only from 1 to 5 mg/m^3

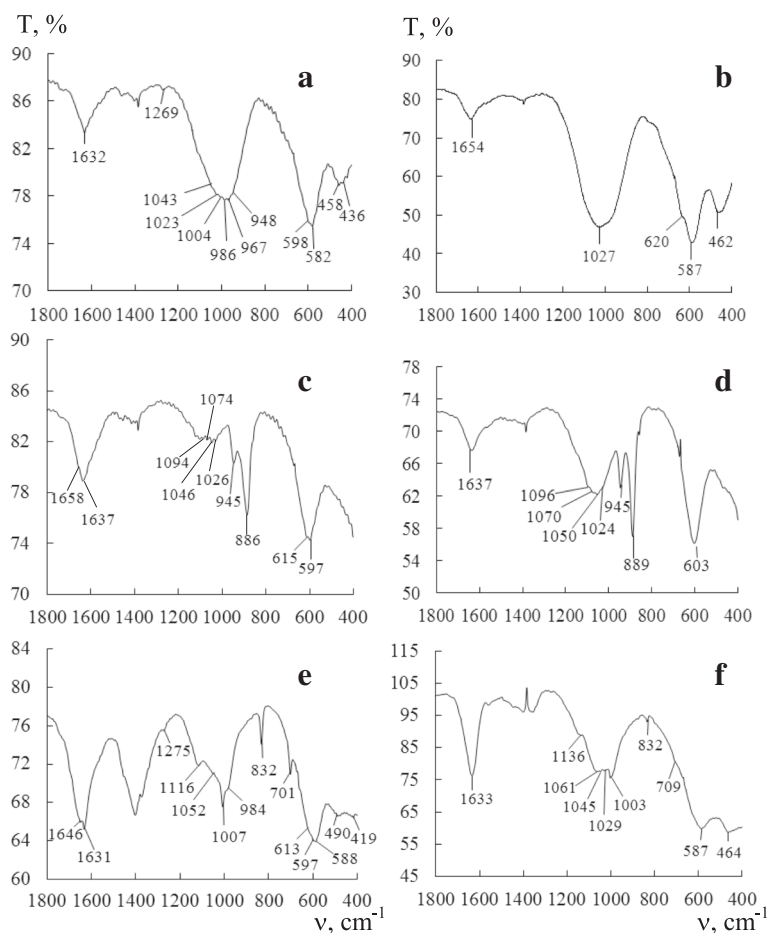


Fig. 2 IR spectra of the freshly prepared (a, c, e) and modified (b, d, f) SCWAs: a, b ANO; c, d TsL; e, f UONI

for FP SCWA-ANO, from 15 to 58 mg/m³ for FP SCWA-TsL, and from 20 to 80 mg/m³ for FP SCWA-UONI.

Modification of SCWA samples causes significant changes in the kinetics of ozone decomposition. M SCWA-ANO and M SCWA-TsL decompose ozone

with attainment of a steady-state mode approximately in 60 min after passing the OAM through the catalyst bed. A curve 2 corresponding to M SCWA-UONI is located lower than the curves for the first two samples; however, no steady-state mode is observed for it. The

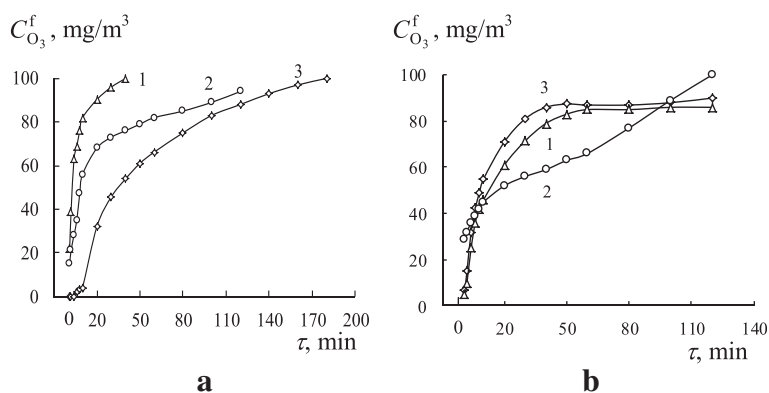


Fig. 3 Time dependences of the final ozone concentration, $C_{O_3}^f$, in the course of ozone decomposition by freshly prepared (a) and modified (b) SCWAs. 1 SCWA-TsL, 2 SCWA-UONI, and 3 SCWA-ANO ($C_{O_3}^i = 100 \text{ mg/m}^3$, $m_s = 0.5 \text{ g}$)

kinetic parameters (W_{in} , k_1 , and $k_{1/2}$) for the reaction of ozone decomposition by the SCWAs under study and amounts of ozone entered into the reaction (Q_{exp}) are summarized in Table 5.

Values of k_1 (calculated for the initial portions of the kinetic curves) and $k_{1/2}$ (calculated at the time of half-conversion of ozone) are not equal being evidence of ozone decomposition proceeding by the radical chain mechanism (much the same as in the case of complex compounds [36, 37], metal oxides [38], etc.). Magnetite, manganochromite, and iron(III) oxides can be considered as catalytically active phases (CAPs) in the reaction of ozone decomposition. All of them contribute to the total catalytic activity of SCWAs, but it is impossible to determine a specific contribution made by each of them.

The highest catalytic activity is demonstrated by SCWA-ANO, both FP and M, characterized by both high phase homogeneity and high CAP contents: 81 and 97 %, respectively. The low catalytic activity for FP SCWA-TsL can be explained not only by its low CAP content of 51 % but also by high contents of impurity phases such as calcium and nickel fluorides and magnesium silicate blocking an access to active sites of the SCWA surface for ozone molecules. Although the CAP contents are practically the same for FP and M SCWA-TsL (Table 4) and there is only a slight difference in the sizes of their Fe_3O_4 nanoparticles, removing water-soluble impurities makes accessible active phases of M SCWA-TsL taking part in the reaction of ozone decomposition and causes the steady-state mode of ozone decomposition (Fig. 3b, curve 1). In the case of FP SCWA-TsL and FP SCWA-UONI, their CAP contents are very close and a bigger activity of the latter in the reaction (Fig. 3a) can be caused by other factors, e.g., by the great difference in the sizes of their ferrite nanoparticles. XRD (Fig. 1f) and IR spectroscopic analysis (Fig. 2f) show that substantial structural changes occurred after modification of SCWA-UONI. These changes resulted in a decrease of kinetic parameters (W_{in} and k_1) (Table 5) characterizing the activity of M SCWA-UONI over the initial period of the reaction.

Table 5 Kinetic parameters for the reaction of ozone decomposition by freshly prepared and modified SCWAs ($C_{O_3}^in = 100 \text{ mg/m}^3$, $m_s = 0.5 \text{ g}$)

Sample	$W_{in} \times 10^8$, mol/L \times s	$k_1 \times 10^3$, s ⁻¹	$k_{1/2} \times 10^4$, s ⁻¹	$Q_{exp} \times 10^5$, O ₃ moles
FP SCWA-ANO	7.00	4.4	3.3	8.3
M SCWA-ANO	6.51	3.7	14.4	4.0
FP SCWA-TsL	5.76	2.2	24.0	0.9
M SCWA-TsL	6.65	3.8	8.8	4.9
FP SCWA-UONI	5.95	2.4	13.8	4.4
M SCWA-UONI	4.97	0.8	6.1	6.0

Conclusion

The samples of SCWAs were obtained as a result of steel welding by three electrodes of Ukrainian manufacture. The phase compositions of the samples, both freshly prepared (FP) and modified (M) by water treatment at 60 °C, were studied by X-ray phase analysis and IR spectroscopy. The results of X-ray phase analysis show that the freshly prepared and modified SCWAs are polyphase systems consisting of magnetite, metal-substituted ferrites, metal oxides, carbonates, and fluorides of alkali and alkaline-earth metals, and chromates. The unit cell parameter and the size of a magnetite nanoparticle (ranging from 15 to 68 nm depending on the chemical composition of an electrode) have been estimated. IR spectral investigations confirm the polyphase composition of the SCWAs. The biggest differences are apparent in the regions of deformation vibrations of M–O–H bonds and stretching vibrations of M–O bonds (M–Fe, Cr). The kinetics of ozone decomposition by FP and M SCWAs at $C_{O_3}^in = 100 \text{ mg/m}^3$ has been studied, and kinetic parameters (W_{in} , k_1 , and $k_{1/2}$) as well as amounts of ozone entered into the reaction have been calculated. The catalytic activity has been found to decrease in the order SCWA-ANO > SCWA-UONI \approx SCWA-TsL corresponding to the decrease in the content of catalytically active phases in their compositions. A low activity of SCWA-UONI and SCWA-TsL is caused by a high content (20–24 %) of the calcium fluoride phase blocking a surface of the catalytically active phases.

Competing Interests

The authors declare that they have no competing interests.

Authors' Contributions

TR analyzed the X-ray diffraction patterns of the SCWA samples, developed the methodology for analyzing kinetic data, and generalized the results obtained. AT took the diffractometer readings, analyzed the IR spectra of all samples, studied the kinetics of ozone decomposition, and made the necessary calculations. AE developed the technique for SCWA preparation and obtained the samples for their further research. WV measured the IR spectra of FP and M SCWAs and translated the manuscript. All authors read and approved the final manuscript.

Authors' Information

TR, a professor, worked as a Head of the Department of Inorganic Chemistry and Chemical Ecology of Odessa I.I. Mechnikov National University. Her research interests are nanochemistry, nanotechnology, coordination chemistry, and catalysis of redox reactions. AT worked as a docent of the Department of Inorganic Chemistry and Chemical Ecology of Odessa I.I. Mechnikov National University. Her research interests are nanochemistry, coordination chemistry, and catalysis of the ozone decomposition reaction. AE, a professor, worked as a Director of the Physicochemical Institute of Environment and Human Protection. His research interests are physicochemical properties of aerosols, engineering of air purification from aerosols, and gaseous toxicants. WV worked as senior researcher at the Department of Inorganic Chemistry and Chemical Ecology of Odessa I.I. Mechnikov National University. Her research interest is environmental catalysis.

Acknowledgements

The study was carried out with the support of the Ministry of Education and Science of Ukraine.

Received: 26 October 2015 Accepted: 1 December 2015

Published online: 09 December 2015

References

- Ennan AA, Rakitskaya TL, Paina VY (1997) Catalysts for low-temperature carbon monoxide oxidation in the process of purification of welding aerosols. *Avtomat svarka* 2:42–44
- Oprya M, Kiro S, Worobiec A, Horemans B, Darchuk L, Novakovic V et al (2012) Size distribution and chemical properties of welding fumes of inhalable particles. *J Aerosol Sci* 45:50–7
- Ennan AA, Kiro SA, Oprya MV, Vishnyakov VI (2013) Particle size distribution of welding fume and its dependency on conditions of shielded metal arc welding. *J Aerosol Sci* 64:103–10
- Voitkevich VG, Bezruk LI, Esaulenko GB (1984) Electron microscopic investigation of the solid component of welding aerosols. *Avtomat svarka* 6:33–5
- Tandon RK, Payling R, Chenhall BE, Crisp RT, Ellis J, Baker RS (1985) Application of X-ray photoelectron spectroscopy to the analysis of stainless-steel welding aerosols. *Appl Surface Sci* 20(4):527–37
- Tanninen VP, Hyvarinen HK, Grekula A, Kalliomaki PL (1985) Experimental improvements in analysis of aerosol samples by X-ray powder diffraction. *J Aerosol Sci* 16(5):373–8
- Kalliomaki RL, Aitio A, Lakomaa EL, Kalliomaki K (1987) Kinetics of the metal components of intratracheally instilled mild and stainless steel welding fumes in parts. *J Aerosol Sci* 18(6):737–40
- Yavdoshin IR, Pokhodnya IK (2002) Formation of a welding aerosol in the process of arc fusion welding and its hygienic evaluation. In: *The book of collected works of 1st Int. Sci. Pract. Conf. "Protection of Environment, Health, and Safety in Welding"*. Astroprint, Odessa, pp 38–56
- Bhamjia I, Preussa M, Threadgill PL, Moata RJ, Addison AC, Peeld MJ (2010) Linear friction welding of AISI 316L stainless steel. *Mater Sci Eng A* 528(2):680–90
- Kumfer BM, Shinoda K, Jayadevan B, Kennedy IM (2010) Gas-phase flame synthesis and properties of magnetic iron oxide nanoparticles with reduced oxidation state. *J Aerosol Sci* 41(3):257–65
- Rakitskaya TL, Truba AS, Ennan AA, Kiro SA, Volkova VY (2014) Nanostructured materials based on the solid component of welding aerosol as catalysts for low-temperature ozone decomposition. In: *The book of Conf. Proceedings Internat. Conf. "Oxide Materials for Electronic Engineering"*. Publishen House of Lvivska Politehnika, Lviv, pp 230–31
- Annoni R, Souza PS, Petrankova M, Miskufova A, Havlik T (2013) Submerged-arc welding slags: characterization and leaching strategies for the removal of aluminum and titanium. *J Hazard Mater* 244–245:335–341
- Rakitskaya TL, Truba AS, Ennan AA, Kiro SA, Volkova VY (2014) Physicochemical and catalytic properties of the solid component of welding aerosol. *Chem Phys Tech Surf* 5(4):396–403
- Rakitskaya TL, Truba AS, Ennan AA, Kiro SA, Volkova VY (2015) Phase composition and catalytic activity of nanostructured materials based on solid component of welding aerosol. *Solid State Phenom* 230:279–84
- Gonzalez-Sandoval MP, Beesley AM, Miki-Yoshida M, Fuentes-Cobas L, Matutes-Aquino JA (2004) Comparative study of the microstructural and magnetic properties of spinel ferrites obtained by co-precipitation. *J Alloys Compounds* 369:190–4
- Zhaola L, Zhanga H, Xinga Y, Songa S, Yua S, Shia W et al (2008) Studies on the magnetism of cobalt ferrite nanocrystals synthesized by hydrothermal method. *J Solid State Chemistry* 181:245–52
- Wei Y, Han B, Hu X, Lin Y, Wang X, Deng X (2012) Synthesis of Fe₃O₄ nanoparticles and their magnetic properties. *Procedia Engineering* 27:632–37
- Albuquerque AS, Tolentino MVC, Ardisson JD, Moura FCC, Mendonca R, Macedo WAA (2012) Nanostructured ferrites: structural analysis and catalytic activity. *Ceram Int* 38:2225–31
- Taseidifara M, Khataee A, Vahidb B, Khorramc S, Joo SW (2015) Production of nanocatalyst from natural magnetite by glow discharge plasma for enhanced catalytic ozonation of an oxazine dye in aqueous solution. *J Mol Catalysis A: Chemical* 404–405:218–26
- Mirkin LI (1961) *Handbook on the X-ray structural analysis of polycrystals*. State Publishing House of Physicomathematical Literature, Moscow, 863 p
- Tang GD, Shang ZF, Zhang XY, Xu J, Lin ZZ, Zhen CM et al (2015) Evidence from infrared spectra for the magnetic moment directions of CR cations in the spinel ferrites. *Physica B* 463:26–9
- Hashemian S, Dehghanpor A, Moghahed M (2014) Cu_{0.5}Mn_{0.5}Fe₂O₄ nano spinels as potential sorbent for adsorption of brilliant green. *J Ind Eng Chem* 24:308–14
- Aphesteguy JC, Kurlyandskaya GV, Celis JP, Safronov AP, Schegoleva NN (2015) Magnetite nanoparticles prepared by co-precipitation method in different conditions. *Mater Chem Phys* 161:243–9
- Khalil MI (2015) Co-precipitation in aqueous solution synthesis of magnetite nanoparticles using iron (III) salts as precursors. *Arabian J Chem* 8(2):279–84
- Wu S, Sun A, Zhai F, Wang J, Xu W, Zhang Q et al (2011) Fe₃O₄ magnetic nanoparticles synthesis from tailings by ultrasonic chemical co-precipitation. *Mater Lett* 65(12):1882–84
- Giri SK, Das NN, Pradhan GC (2011) Synthesis and characterization of magnetite nanoparticles using waste iron ore tailings for adsorptive removal of dyes from aqueous solution. *Coll Surf A: Physicochem Eng Aspects* 389:43–9
- Hosseini-Monfared H, Parhegani F, Alavi S (2015) Carboxylic acid effects on the size and catalytic activity of magnetite nanoparticles. *J Coll Interf Sci* 437:1–9
- Ivanovskaya MI, Tolstik AI, Kotikov DA, Pan'kov VV (2009) Structural features of Zn-Mn-ferrite synthesized by the spray-type pyrolysis method. *Zhurn Fiz Khimii* 83(12):2283–8
- Salazar-Camacho C, Villalobos M, Luz R-SM, Arenas-Alatorre J, Alcaraz-Cienfuegos J, Gutierrez-Ruiz ME (2013) Characterization and surface reactivity of natural and synthetic magnetites. *Chem Geology* 347:233–45
- Morel M, Martinez F, Mosquera E (2013) Synthesis and characterization of magnetite nanoparticles from mineral magnetite. *J Magnetism Magnetic Mater* 343:76–81
- Nakamoto K (1991) *IR and Raman spectra of inorganic and coordination compounds*. Mir, Moscow, p 536
- Davydov AA (1984) *IR spectroscopy in the surface chemistry of oxides*. Nauka, Novosibirsk, 245 p
- Burgina EB, Kustova GN, Tsybulya SV, Kryukova GN, Litvak GS, Isupova LA et al (2000). Features of the structure of metastable modifications of iron(III) oxide. *Zhurn. Strukturnoy Khimii* 41(3):489–97
- Calero-DdelC VL, Rinaldi C (2007) Synthesis and magnetic characterization of cobalt-substituted ferrite (Co_xFe_{3-x}O₄) nanoparticles. *J Magnetism Magnetic Mater* 314:60–7
- Kumar R, Sakthivel R, Behura R, Mishra BK, Das D (2015) Synthesis of magnetite nanoparticles from mineral waste. *J Alloys and Compounds* 645:398–404
- Rakitskaya TL, Ennan AA, Granatyuk IV, Bandurko AY, Balavoine GGA, Geletii YV et al (1999) Kinetics and mechanism of low-temperature ozone decomposition by Co-ions adsorbed on silica. *Catal Today* 53(4):715–23
- Rakitskaya TL, Truba AS, Raskola LA, Radchenko EA, Strizhak AV, Golub AA (2013) Antiozonant activity of the silica modified with 3d-metal complexes. *Rus J Gen Chem* 83(2):360–7
- Oyama ST (2000) Chemical and catalytic properties of ozone. *Catal Rev Sci Eng* 42(3):279–322

Submit your manuscript to a SpringerOpen® journal and benefit from:

- Convenient online submission
- Rigorous peer review
- Immediate publication on acceptance
- Open access: articles freely available online
- High visibility within the field
- Retaining the copyright to your article

Submit your next manuscript at ► springeropen.com